Bioactive Materials 38 (2024) 169–180

Contents lists available at ScienceDirect

Bioactive Materials

journal homepage: www.keaipublishing.com/en/journals/bioactive-materials

Regulating the bioactivity of non-glycosylated recombinant human bone morphogenetic protein-2 to enhance bone regeneration

Yuanman Yu [a,b,c,1,**], Rui Chen [a,b,1], Xinye Chen [a,c], Jing Wang [a,b,c,*], Changsheng Liu [b,c,***]

[a] The State Key Laboratory of Bioreactor Engineering, East China University of Science and Technology, Shanghai, 200237, PR China
[b] Key Laboratory for Ultrafine Materials of Ministry of Education, Engineering Research Center for Biomedical Materials of Ministry of Education, School of Materials Science and Engineering, East China University of Science and Technology, Shanghai, 200237, PR China
[c] Frontiers Science Center for Materiobiology and Dynamic Chemistry, East China University of Science and Technology, Shanghai, 200237, PR China

ARTICLE INFO

Keywords:
Recombinant human bone morphogenetic protein-2
Osteogenic activity
Protein stability
Sulfated polysaccharide

ABSTRACT

Recombinant human bone morphogenetic protein-2 (rhBMP-2) is the predominant growth factor that effectively induces osteogenic differentiation in orthopedic procedures. However, the bioactivity and stability of rhBMP-2 are intrinsically associated with its sequence, structure, and storage conditions. In this study, we successfully determined the amino acid sequence and protein secondary structure model of non-glycosylated rhBMP-2 expressed by an *E. coli* expression system through X-ray crystal structure analysis. Furthermore, we observed that acidic storage conditions enhanced the proliferative and osteoinductive activity of rhBMP-2. Although the osteogenic activity of non-glycosylated rhBMP-2 is relatively weaker compared to glycosylated rhBMP-2; however, this discrepancy can be mitigated by incorporating exogenous chaperone molecules. Overall, such information is crucial for rationalizing the design of stabilization methods and enhancing the bioactivity of rhBMP-2, which may also be applicable to other growth factors.

1. Introduction

Bone morphogenetic protein 2 (BMP-2) is a classical member of the transforming growth factor-β superfamily, acting as a potent regulator to induce bone formation [1–3]. Given its excellent osteoinductive ability, BMP-2 has been approved by the Food and Drug Administration (FDA) for clinical applications in different bone repair situations [4]. Till now, high purity recombinant human BMP-2 (rhBMP-2) can be mass-produced with various expression systems including eukaryotic expression in mammalian cell cultures [5] and prokaryotic expression in bacteria [6]. The glycosylated rhBMP-2 (G-rhBMP-2) is considered to exhibit enhanced biological activity due to its high solubility resulting from N-linked glycosylation [7], a post-translational modification. However, the inclusion of serum in mammalian cell culture significantly escalates the production cost of glycosylated rhBMP-2. In contrast, the non-glycosylated rhBMP-2 (NG-rhBMP-2) expressed by the prokaryotic system distinguishes itself with its advantages of economic feasibility and exceptional yield. However, the stability and biological activity of NG-rhBMP-2 are inferior to those of G-rhBMP-2, posing an urgent challenge in its practical application.

The biological activity of proteins is closely related to its stability and structure, various factors such as solution pH, temperature conditions, and shear stress can lead to structural changes in proteins during the preparation and storage of rhBMP-2 [8–10]. Thereinto, protein aggregation is one of the main factors that reduce its stability, inhibit the biological activity, and eventually lead to protein precipitation. In addition, protein aggregates can also trigger non-specific activation of receptor molecules, leading to reduced bioactivity and high toxicity [11]. Therefore, optimization of preparation and storage conditions to reduce protein aggregation continues to be a pressing priority in maintaining the bioactivity of rhBMP-2. Accumulated evidences suggested that formulation pH plays an important role in protein aggregation [12,

Peer review under responsibility of KeAi Communications Co., Ltd.
* Corresponding author. The State Key Laboratory of Bioreactor Engineering, East China University of Science and Technology, Shanghai, 200237, PR China.
** Corresponding author. The State Key Laboratory of Bioreactor Engineering, East China University of Science and Technology, Shanghai, 200237, PR China.
*** Corresponding author. Key Laboratory for Ultrafine Materials of Ministry of Education, Engineering Research Center for Biomedical Materials of Ministry of Education, School of Materials Science and Engineering, East China University of Science and Technology, Shanghai, 200237, PR China.
E-mail addresses: ymyu@ecust.edu.cn (Y. Yu), wangjing08@ecust.edu.cn (J. Wang), liucs@ecust.edu.cn (C. Liu).
[1] These authors contributed equally to this work.

https://doi.org/10.1016/j.bioactmat.2024.04.018
Received 29 November 2023; Received in revised form 15 April 2024; Accepted 16 April 2024

13]. Given the most proteins are amphoteric molecules, any alteration in the pH of the medium will inevitably impact the net charge on the protein surface, thereby influencing the balance between attractive and repulsive forces among proteins. Consequently, this can lead to significant changes in pH within the BMP-2 system, subsequently affecting both stability and biological activity of rhBMP-2. These limitations serve as motivation for investigating the correlation between pH and bioactivity of rhBMP-2 to enhance its efficacy in bone healing.

An alternative strategy for enhancing protein activity involves the incorporation of molecular chaperone, which optimize their biological functionality by finely modulating the exposure of active sites within their protein conformation. For example, fibronectin (Fn) has the capability to augment the bioactivity of rhBMP-2 by instigating synergistic signaling between growth factor receptors and integrins [14,15]. The co-immobilization of both rhBMP-2 and collagen type I (Col-I) can expedite the osteogenesis process of mesenchymal stem cells (MSCs) [16,17]. Heparin (Hep) possesses the ability to regulate the biological activity of rhBMP-2 through its heparin binding domain, thereby enhancing its osteogenic potential [18–20]. Furthermore, our previous studies have documented a semi-synthesized sulfated chitosan (SCS) that efficiently enhances the osteogenic activity of rhBMP-2 via activating the phosphorylation of BMP-2 receptors [21]. However, the differences in the capacity of various molecular chaperones to enhance NG-rhBMP-2 activity and whether they can augment NG-rhBMP-2 activity to a level comparable with that of G-rhBMP-2 activity remain unknown.

Due to the poor solubility of NG-rhBMP-2, its biological activity is significantly affected during application. To address this issue, our group has independently designed and optimized the relevant sequences of BMP-2 previously, resulting in the successful preparation of highly bioactive NG-rhBMP-2 [22]. In this study, we performed a comparative analysis of its structural variances of NG-rhBMP-2 (prepared by our group) with the theoretical model (data from Protein Data Bank). We further examined the impact of varying pH storage conditions on both the structural integrity and biological efficacy of NG-rhBMP-2. Additionally, to elucidate the distinct biological functions between G-rhBMP-2 and NG-rhBMP-2, we comprehensively examined their effects on osteogenesis, osteoclastogenesis, and angiogenesis during bone formation. We also explored the potential of various molecular chaperones (e.g., Col I, Fn, Hep, and SCS) to enhance the osteogenic activity of NG-rhBMP-2, with the expectation that they could attain a level of activity comparable to G-rhBMP-2. We hypothesize these results of our systematic study may provide compelling evidence for the preservation of NG-rhBMP-2 activity throughout isolation and formulation processes while enhancing its clinical promotion and application.

2. Results and discussion

2.1. Construction and molecular structure analysis of NG-rhBMP-2

To validate the biological activity of *E. coli*-expressed rhBMP-2, we initially conducted an analysis of its amino acid sequence and structure. The X-ray crystal structure analysis is a highly effective method for analyzing protein structures, with the key to accurate analysis lying in obtaining well-formed protein crystals. Therefore, in order to optimize the crystallization conditions and obtain higher quality rhBMP-2 crystals (Fig. S1), we first optimized and screened the pH value of the reservoir solution and protein solution, protein concentration, and salt concentration (ionic precipitator).

The formation of proteins occurs through the condensation of multiple amino acids and their classification as amphoteric electrolytes renders them highly sensitive to the pH level of the crystallization solution [23,24]. Adjusting the pH value can consequently alter both the size and shape of protein crystals, thereby constituting a crucial factor that influences the protein crystallization process. The results revealed that the formation of rhBMP-2 crystals occurred within a pH range of 5.0–5.6, whereas an increase in the reservoir liquid's pH to 6.0 resulted in minimal growth of rhBMP-2 crystals (Fig. S2). In addition, the pH of the protein plays a crucial role in facilitating the formation of protein crystals. The results from rhBMP-2 crystal culture demonstrated an accelerated precipitation rate with increasing pH values within the range of 3.0–4.0, while the formation rate of rhBMP-2 crystals was slow and challenging (Fig. S3).

We also investigated the effect of protein concentration on protein crystal formation. The results demonstrate that an increase in protein concentration within the range of 1.0–3.0 mg/mL leads to accelerated precipitation rate, enhanced crystal appearance rate, and increased crystal size (Fig. S4). The protein crystals observed in the experimental group with a concentration of 1.0 mg/mL rhBMP-2 measured approximately 80 μm × 80 μm × 60 μm; whereas those in the group with a concentration of 2.0 mg/mL were around 200 μm × 200 μm × 150 μm; and finally, almost complete precipitation was observed in the group with a concentration of 3.0 mg/mL. Furthermore, it was found that concentrations below 1 mg/mL failed to yield any rhBMP-2 crystals within a period of four weeks. These findings indicate that protein concentration significantly influences both the formation rate and size of rhBMP-2 crystals. The addition of salt precipitants, such as ionic precipitant Li_2SO_4, can disrupt the hydration layer surrounding proteins, thereby diminishing their affinity for water and enhancing intermolecular binding to facilitate crystal formation [25]. Experimental findings demonstrate that rhBMP-2 crystals fail to form in the absence of added salt, while concentrations ranging from 25 to 75 mM exhibit minimal crystallization. Notably, consistent crystal formation is observed within the concentration range of 100–150 mM (Fig. S5). Furthermore, an increase in salt concentration correlates with a higher probability of microcrystal occurrence. These results underscore the indispensable role of Li_2SO_4 as a crucial precipitating agent for promoting rhBMP-2 crystallization. The comprehensive screening outcome of rhBMP-2 crystallization was documented in Table S1.

The diffraction pattern of the rhBMP-2 crystal is obtained through X-ray diffraction of 2.6–2.9 Å. The space group of rhBMP-2 is R32, which belongs to the tripartite system, and its cell parameters are $a = b = 94.21$ Å, $c = 101.58$ Å, $\alpha = \beta = 90°$, $\gamma = 120°$ (Fig. 1a). Upon comparison with specific structural parameters of the model protein (Protein Data Bank code: 3BMP) [26], it was observed that both rhBMP-2 crystal space groups belonged to R32, with a total of 3732 and 4645 data sets respectively utilized for meticulous structural analysis, indicating an exceptional level of integrity (Table S2). R_{cryst} serves as an invaluable indicator for assessing the accuracy of the modified protein structure by quantifying discrepancies in diffraction point amplitudes between observed and calculated values. Typically, an acceptable R_{cryst} value after most corrections hovers around approximately 20 %, whereas in our experimental group it measures approximately at a slightly higher but still commendable rate of about 20.7 %, thus unequivocally confirming the veracity and precision achieved in rhBMP-2's structural analysis.

The three-dimensional structure of rhBMP-2 was reconstructed using PyMOL software, revealing that compared to the PDB-reported rhBMP-2, amino acid residues No. 1–11 at the N-terminal were not visible in the experimental group, while only residues No. 1–8 were invisible in the protein library rhBMP-2. This suggests that the N-terminal peptide chain of rhBMP-2 in the experimental group may exhibit enhanced motor activity (Fig. 1b). Both rhBMP-2 sequences are identical and derived from amino acids No. 283–396 encoded by gene P12643. In comparison to the secondary structure reported in literature, rhBMP-2 in the experimental group possesses an additional α-helix (23Phe - 26Val) and a longer β-folded segment (β5 - β8), indicating a potentially more compact molecular structure for rhBMP-2 in this setting (Fig. 1c). Together, these results suggest that the molecular structure of rhBMP-2 expressed by *Escherichia coli* was consistent with the primary structure documented in the PDB, while exhibiting similarities in both secondary and spatial conformation.

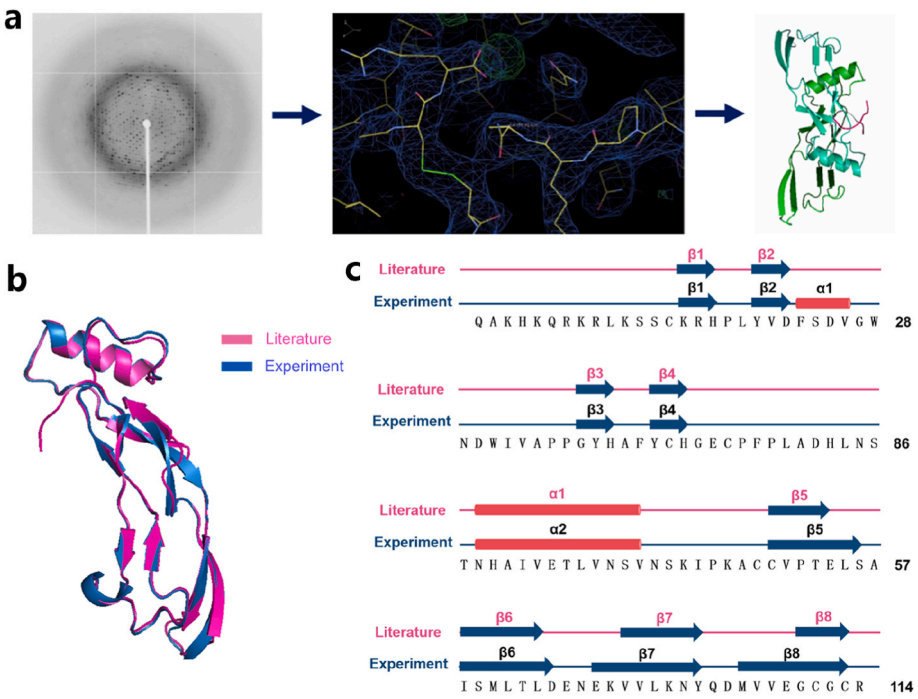

Fig. 1. Molecular structure of *E. coli*-derived rhBMP-2. (**a**) The data processing flowchart of rhBMP-2 crystals. The X-ray diffraction analysis was performed to obtain the diffraction pattern of rhBMP-2. (**b**) Comparative analysis of the folding topology between the experimental group rhBMP-2 and the model group rhBMP-2 (PDB code: 3BMP). (**c**) Comparisons of the amino sequences and secondary structures of the experimental group rhBMP-2 and the model group rhBMP-2: blue arrows and red cylinders represent β-sheets and α-helix, respectively.

2.2. Effect of formulation pH on rhBMP-2-induced osteogenesis

In addition to its structural composition, the biological activity of proteins is intricately linked to solution pH, which can induce alterations in protein structure during the preparation and storage of rhBMP-2. To clarify the effect of formulation pH on the aggregation of rhBMP-2, we analyzed the diameter of protein at different formulation pH conditions. Z-average diameter analysis revealed that the rhBMP-2 exhibited a smallest particle size (~130 nm) at the formulation pH condition of 4.5 (Fig. 2a) compared to the other groups, indicating that the rhBMP-2 particles did not occur significant aggregation. The particle size of rhBMP-2 gradually increased with the formulation pH conditions becoming alkaline, and reached its maximum value of 300 nm at pH 6.5 (Fig. 2a). Additionally, zeta potential measurements showed that rhBMP-2 had a positive charge under acidic conditions, while it transferred to negative charge under alkaline conditions (Fig. 2b). As rhBMP-2 is an acidic protein, the hydrogen ions could be easily adsorbed on the surface of protein under acidic conditions, which induce an intermolecular repulsion between rhBMP-2 to reduce the protein aggregation [27]. With the increase of pH value, the surface charge of rhBMP-2 was neutralized and the intermolecular repulsion between proteins was disappeared. Particularly, zeta potential measurements revealed that the rhBMP-2 at the formulation pH condition of 6.5 exhibited a neutral charge, which weakened the intermolecular repulsion and resulted to a serious aggregation and precipitation of rhBMP-2.

We further investigated the difference of protein aggregation of rhBMP-2 at different formulation pH conditions using a quartz crystal microbalance with dissipation monitoring (QCM-D) measurement. An obvious reduction in frequency was detected with the initial injection of rhBMP-2 into the QCM-D chamber (Fig. S6a). However, a significant difference in Δf was observed among the experimental groups. The Δf of rhBMP-2 at the adsorption equilibrium states was 23.5 ± 0.6 at the formulation pH value of 4.5 (Fig. S6b). As the buffer changed from acidic to alkaline, the detected Δf gradually increased and reached a maximum at pH 6.5. Additionally, a specific $\Delta D/\Delta f$ value was calculated to show the induced energy dissipation per unit detected mass (Fig. S6c). The result suggested that a mass uptake on the surface induced a significant increase in dissipation, which correlates to a viscoelastic surface film. Thus, we further calculated the adsorbed mass of rhBMP-2 using a Voigt-based viscoelastic model. As depicted in Figs. S6d and a smallest weight change about 426.0 ± 10.6 ng/cm^2 could be observed when rhBMP-2 stored at the buffer of pH 4.5. With the increasing value of pH, the saturated adsorption capacity of rhBMP-2 gradually increased and reached a peak at pH 6.5 (~1844.3 ± 62.0 ng/cm^2). This was mainly attributed to the high aggregation of rhBMP-2 at the pH 6.5 condition. Together, the results suggest that rhBMP-2 in an acid condition is more stable relative to neutral and alkaline conditions.

To further determine the structural stability of rhBMP-2 at different formulation pH conditions, circular dichroism (CD) spectroscopy analysis was used to calculate the secondary structure compositions (% α-helix, β-sheet, β-turn, and random coil) of rhBMP-2 in the solution. CD spectra analysis showed that the secondary structures of rhBMP-2 were relatively stable in acidic condition, the percentage of α-helix, β-sheet, β-turn, and random coil structures of rhBMP-2 at the formulation pH value of 4.5 and 5.5 was 13.0 %, 25.6 %, 17.8 %, and 43.6 %, respectively (Fig. 2c and d). As the buffer changed from acidic to alkaline, the proportion of β-sheet structure significantly increased, while the proportion of random coil structure gradually decreased. Typically, when rhBMP-2 was stored at the solution of formulation pH value of 8.5, the α-helix and β-sheet structure of rhBMP-2 increased to 15.7 % and 29.7 %, while the random coil structure decreased to 36.9 % (Fig. 2d). This result suggests that the formulation pH condition plays an important role in the regulation of secondary structure of rhBMP-2.

Molecular fluorescence spectroscopy is an effective technique to establish conformational modifications and protein interactions in solution because of its good selectivity and high sensitivity. Tryptophan (Trp), tyrosine (Tyr), and phenylalanine (Phe) are the fundamental fluorophores existing in any protein [28,29]. Steady-state fluorescence spectroscopy analysis showed that the emission spectra of rhBMP-2 at different formulation pH showed a well-defined peak centered at 340

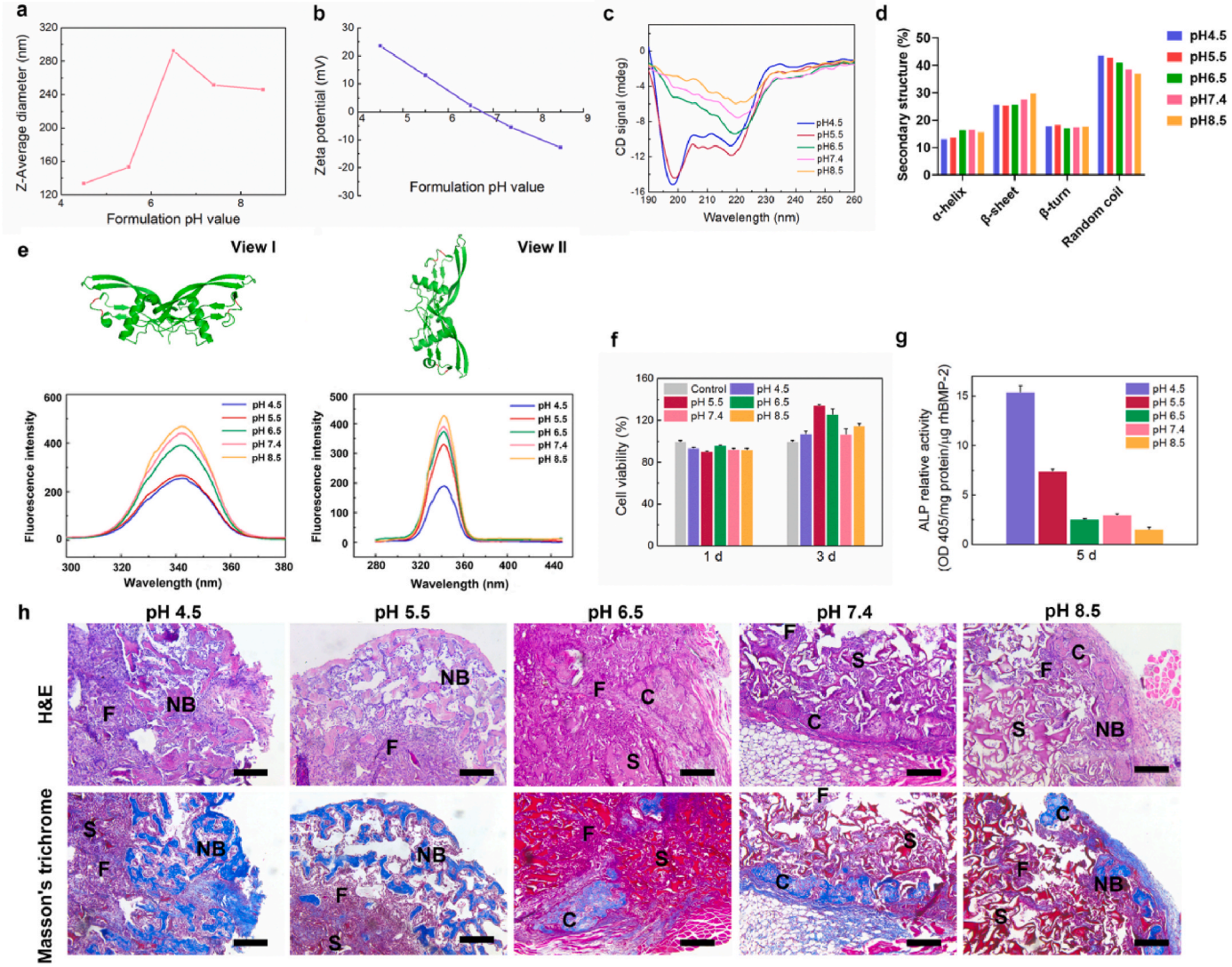

Fig. 2. Influence of formulation pH **on the stabilization and bioactivity of *E. coli*-derived rhBMP-2. (a–b)** Z-average diameter (a) and ζ-potential (b) of rhBMP-2 molecule at different formulation pH conditions. (**c–d**) CD signal spectra of rhBMP-2 (c) and quantifiaction analysis (d) at different formulation pH conditions. (**e**) Fluorescence spectroscopy analysis of rhBMP-2. (**f**) Cell viability of rhBMP-2 aggregates formed at different formulation pH conditions. (**g**) ALP relative activity normalized to the mass of rhBMP-2. (**h**) Histological assessment of H&E staining and Masson's trichrome staining was performed to evaluate rhBMP-2-induced ectopic bone formation under varying formulation pH conditions. RhBMP-2 amount: 10 μg. Scale bars, 100 μm.

nm corresponding to Trp emission, which exhibited no obvious difference among the experimental groups (Fig. 2e). However, with the increasing value of formulation pH, the emission intensities (Imax) of rhBMP-2 significantly increase accompanied by a marginal blue shift (λ_{em}max) of ~1 nm (Fig. 2e and Table 1). The blue shift of emission maximum indicated the polarity attenuation surrounding the Trp microenvironment. Next, we adopted synchronous fluorescence spectroscopy to further investigate the microenvironmental and conformational alteration around Trp in rhBMP-2 at different formulation pH conditions. Similar to the results of steady-state fluorescence spectroscopy analysis, a well-defined peak appeared at 340 nm in all groups (Fig. 2e). With the increasing value of formulation pH, the emission intensities (Imax) of rhBMP-2 significantly increase from 342.8 nm to 341.0 nm accompanied by a marginal blue shift (λ_{em}max) of ~1.8 nm (Table 1).

Previous studies demonstrated that the maximum emission wavelength (λ_{em}max) in molecular fluorescence spectroscopy was always associated with the solvent microenvironment in which Trp residues located [28,30]. When λ_{em}max was above 330 nm, it indicated that Trp residues were exposed in a polar environment and located in the surface layer of the protein molecule. On the contrary, the Trp residue was considered to be located in a non-polar environment inside the protein molecule. In this study, the λ_{em}max of the Trp residues measured by the fluorescence spectra was between 341 nm and 343 nm, indicating that the λ_{em}max was in a polar environment, which was consistent with the observation of the three-dimensional structure of rhBMP-2 (Fig. 2e). In addition, a marginal blue shift of Trp in rhBMP-2 occurred with the increasing value of formulation pH, indicating that the Trp residue was deeply buried inside the cavity of the protein, and the surrounding

Table 1
Fluorescence parameters of steady-state fluorescence spectra (a) and synchronous fluorescence spectra (b) of rhBMP-2 at different formulation pH conditions (Imax: maximum fluorescence intensity, λ_{em}max: maximum emission wavelength).

Group	pH 4.5	pH 5.5	pH 6.5	pH 7.4	pH 8.5
Imax (a)	254.5	267.0	390.5	439.3	468.1
λ_{em}max (a)	342.2	342.0	342.0	341.8	341.2
Imax (b)	189.9	330.0	372.6	389.5	426.3
λ_{em}max (b)	342.8	342.4	341.8	341.6	341.0

microenvironment was less polarity and greater hydrophobicity [31]. However, Trp residue itself was a non-polar group with great hydrophobicity. The entrapment of Trp residue made the surface of rhBMP-2 molecules more hydrophilic, which may lead to changes in the function of rhBMP-2. These results suggest that the different formulation pH conditions will result in the structural change of rhBMP-2. RhBMP-2 stored in alkaline condition can not only lead to protein aggregation, but also in structural changes that lead to loss of biological activity.

Previous studies provide added evidence that the aggregation of proteins can be inherently highly cytotoxic [11]. To investigate the effect of protein aggregation on the cell viability, we anchored the rhBMP-2 on the Au chips with the injection of different pH buffer as mentioned above, and further examined the cell viability of C2C12 with the treatment of rhBMP-2 at different formulation pH conditions on day 1 and day 3. The results indicated that rhBMP-2 in all experimental groups exhibited a favorable cell viability on C2C12 cells on both day 1 and day 3 (Fig. 2f). Over time, the cell number progressively increased with the treatment of rhBMP-2, and rhBMP-2 at pH 5.5 appeared to have the most excellent ability to promote cell proliferation. Additionally, we further assessed the alkaline phosphatase (ALP) expression of C2C12 cells in response to rhBMP-2 induction at different formulation pH conditions. The rhBMP-2 at pH 4.5 exhibited a highest level in osteoinductive activity relative to the other groups. With the increase of pH, the osteogenic activity of rhBMP-2 per unit mass gradually decreased (Fig. 2g). These results indicate that the aggregation of rhBMP-2 decreases the activity of rhBMP-2.

To investigate the storage stability of rhBMP-2 under varying formulation pH, the bioactivity of rhBMP-2 was assessed following storage at different formulation pH for a specified duration. As the storage time increased, a significant decline in ALP quantitative detection was observed (Fig. S7). The highest expression of ALP with respect to rhBMP-2 was observed when stored at pH 4.5, indicating that this condition better preserved the biological activity of rhBMP-2 over time. However, after 28 days of storage, the activity of rhBMP-2 decreased in all groups, suggesting that it should be utilized within two weeks irrespective of the pH conditions. Furthermore, in order to further investigate the bone-inducing activity of rhBMP-2 under varying pH conditions, we conducted a comparative analysis of its osteogenic potential using a well-established ectopic osteogenesis model generated in the hind limb muscle bag of mice. H&E staining analysis showed that a denser trabecular bone could be observed with the treatment of rhBMP-2 stored at pH 4.5 and pH 5.5 (Fig. 2h). In contrast, the trabecular bone formation in the other groups was clearly less pronounced, and cartilage formation occurred instead. Since BMP-2-induced osteogenesis via a classic endochondral ossification, residual cartilage tissue represented a slowing of the bone-induction process. In addition, Masson trichrome analysis also showed that rhBMP-2 stored at an acidic condition exhibited a higher bioactivity compared to that in neutral or alkaline conditions. Specially, the group of pH 4.5 exhibited a greater area of collagen-richen trabecular bone that stained with a navy-blue color, while the groups of pH 7.2 and pH 8.5 showed a greater area of chondrocytes that stained with a pale color (Fig. 2h). These results suggest that rhBMP-2 stores at acidic condition can better maintain its osteogenic activity in vivo.

2.3. Effect of glycosylation modification on osteogenic activity of rhBMP-2

Previous studies have indicated that native BMP-2 and its recombinant counterparts produced in mammalian cells undergo post-translational modifications via N-linked glycosylation [7], which is a crucial factor influencing the solubility and bioactivity of BMP-2. In contrast, bacterially produced BMP-2 lack this glycosylation, resulting in reduced solubility. To compare the osteogenic activity of G-rhBMP-2 and NG-rhBMP-2, we initially examined their impact on ALP expression in C2C12 cells. In the low concentration range, an increase in protein concentration led to a corresponding elevation in ALP activity of both rhBMP-2 induced by C2C12 cells (Fig. 3a), indicating a clear dose-dependent relationship for the in vitro osteogenic activity of NG-rhBMP-2 and G-rhBMP-2. However, G-rhBMP-2 exhibited superior in vitro osteogenic activity when used at equivalent concentrations (Fig. 3a).

The Smad1/5/9 is the classical signaling pathway by which rhBMP-2 transduces signals to the nucleus, thereby coordinating the transcriptional regulation and expression of osteogenic genes [32]. Compared to the Control group, NG-/G-rhBMP-2 treatment induces up-regulation of p-Smad1/5/9 and Runx2 expression levels, indicating activation of the intracellular Smad signaling pathway by NG-/G-rhBMP-2 and subsequent signal transduction to the nucleus. Quantitative analysis reveals a significant increase in p-smad1/5/9 and Runx2 expression levels in the NG-/G-rhBMP-2 group, with no significant difference observed in total Smad1/5/9 protein expression. Moreover, the relative intensity of p-smad1/5/9 is higher in the G-rhBMP-2 group compared to the NG-rhBMP-2 group. Additionally, we conducted an investigation into the expression of osteogenic genes induced by rhBMP-2 at various time intervals. QPCR analysis revealed a significant up-regulation of ALP and OCN gene expression on day 3 and day 7 upon rhBMP-2 induction. Specifically, the expression of ALP gene was significantly increased at day 3 but decreased at day 7, while the expression of OCN gene reached its peak at day 7. Moreover, compared to the NG-rhBMP-2 group, the G-rhBMP-2 group exhibited a significant enhancement in both ALP and OCN gene expression levels. These findings provide compelling evidence for the superior osteogenic activity of G-rhBMP-2 at the genetic level.

To further elucidate the disparity in pro-osteogenic activity between NG-rhBMP-2 and G-rhBMP-2, we conducted additional investigations into the osteoinductive potential of these rhBMPs using a mouse ectopic bone model. The in vivo X-ray imaging and digital photographs revealed the presence of heterotopic bone formation in both NG-rhBMP-2- and G-rhBMP-2-treated groups. However, there was no significant change observed in the size of ectopic bone generated at 2 weeks and 4 weeks (Fig. 4a and b). The wet weight results revealed no significant difference between G-rhBMP-2 and NG-rhBMP-2 after 2 weeks, while the G-rhBMP-2 group exhibited a slight increase in wet weight at 4 weeks (Fig. 4c). Conversely, the ash weight of G-rhBMP-2-induced ectopic bone was higher than that of the NG-rhBMP-2 group at both 2 and 4 weeks, indicating a greater capacity of G-rhBMP-2 to induce new bone formation (Fig. 4d). These findings were further bolstered by the analysis conducted using SRμCT (Fig. 4e and f).

Masson's trichrome staining revealed that both rhBMP-2 groups exhibited dense interconnected bone trabecular structures forming islands at 2 weeks, with abundant presence of bone marrow tissues between the trabeculae (Fig. 4g). Moreover, the G-rhBMP-2 group displayed larger trabeculae compared to the NG-rhBMP-2 group. By 4 weeks, both groups experienced bone resorption, characterized by adipocyte-filled vesicles within the ectopic bone and a reduction in the number of trabeculae along with their increased dispersion (Fig. 4g). These experimental observations align well with the findings obtained from ectopic ash reweighing. Previous studies have reported that the administration of a high dose of rhBMP-2 is invariably associated with the activation of osteoclasts, thereby leading to bone resorption [33,34]. To investigate the impact of two types of rhBMP-2 on osteoclast activation during the initiation of bone formation, we utilized tartrate-resistant acid phosphatase (TRAP) staining to identify and label osteoclasts in rhBMP-2-induced heterotopic bone. The TRAP staining revealed the presence of osteoclasts surrounding the trabecular bones in both groups (Fig. 4h). Comparatively, the NG-rhBMP-2 exhibited a larger TRAP-positive area, indicating a higher number of osteoblasts and increased bone absorption activity (Fig. 4h). Together, these results suggest that G-rhBMP-2 exhibits superior osteoinductive activity compared to NG-rhBMP-2.

Angiogenesis is essential for orchestrating the process of new bone formation [35]. Previous studies have also demonstrated the angiogenic

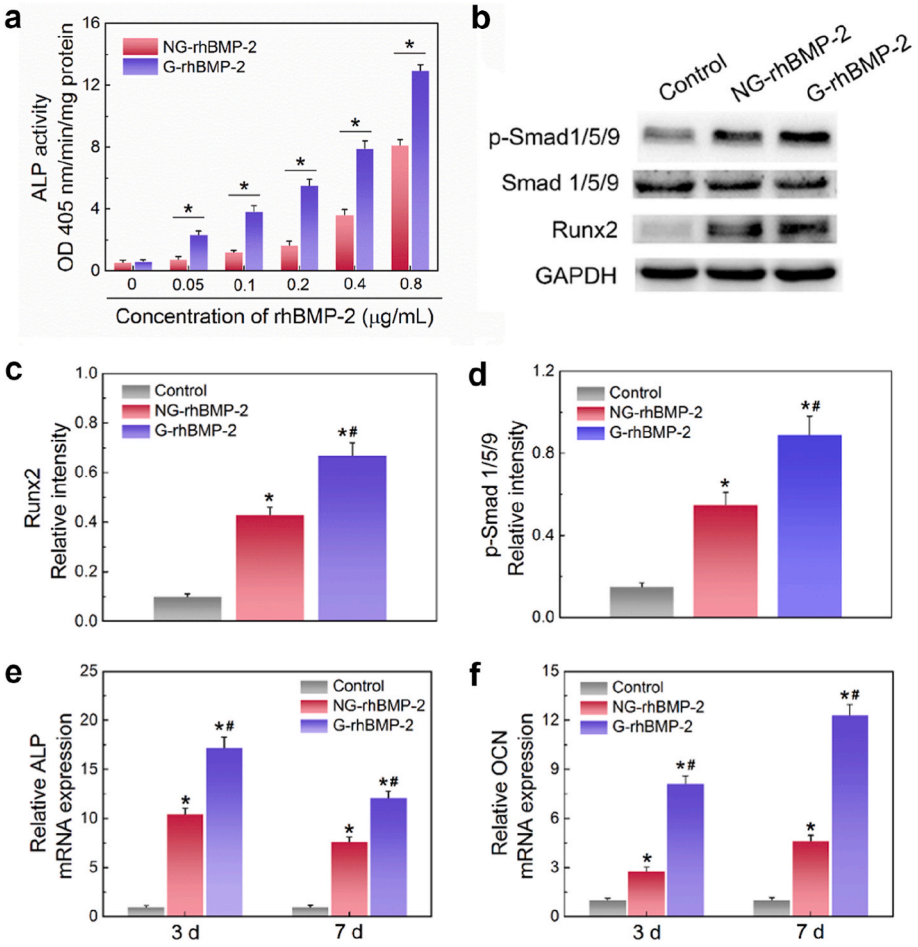

Fig. 3. Comparative analysis of osteogenic activity variations in rhBMP-2 derived from diverse sources. (**a**) ALP activity was detected in C2C12 cells cultured with different concentrations of NG-rhBMP-2 and G-rhBMP-2 for 3 days (n = 3). (**b–d**) Representative electrophoresis images were visualized using ECL plus reagents (b), and the relative intensities of target proteins normalized to GAPDH are shown in (c–d). (**e–f**) The expression levels of gene markers ALP (e) and OCN (f) were measured in C2C12 cells cultured with NG-/G-rhBMP-2 after 3 and 7 days (n = 3). NG-rhBMP-2 and G-rhBMP-2 denote rhBMP-2 that lacks glycosylation and rhBMP-2 that is glycosylated, respectively. $^{*}P < 0.05$ and $^{\#}P < 0.05$ represent statistically significant difference compared with Control and NG-hBMP-2 group, respectively.

potential of rhBMP-2 [36–38]. Therefore, we further compared the angiogenic capabilities between NG-rhBMP-2 and G-rhBMP-2. SRμCT analysis revealed the presence of well-defined blood vessels in both groups of ectopic bones, forming an interconnected vascular network at 2 weeks (Fig. 4i). Notably, there was no significant disparity observed in the quantity of blood vessels between the two groups (Fig. 4j). Immunohistochemical staining revealed that the expression of CD31 surrounding the bone trabeculae in both groups of ectopic bone samples, exhibiting a distinctive brown ring structure indicative of blood vessel presence (Fig. S8). Furthermore, within the ring area, distinct red blood cells were observed, suggesting that these newly formed capillaries possess functional capabilities for nutrient and oxygen transport (Fig. S8). These results suggest that both NG-rhBMP-2 and G-rhBMP-2 demonstrate remarkable efficacy in promoting neovascular growth, exhibiting no discernible disparity between them.

2.4. SCS enhanced NG-rhBMP-2-induced osteogenesis

Accumulating evidence suggests that the osteoinductive activity of rhBMP-2 can be enhanced through controlled release of the carrier [39,40], regulation of protein conformation [41,42], and exposure of the protein's active site [21] et al. Consequently, the incorporation of chaperone molecules into NG-rhBMP-2 is expected to augment its osteoinductive activity while simultaneously ensuring cost-effectiveness. To evaluate the potential of chaperone molecules in augmenting the bioactivity of NG-rhBMP-2, we introduced four specific chaperones - collagen I (Col-I), fibronectin (Fn), heparin (Hep), and sulfated chitosan (SCS) - and examined their impact on rhBMP-2-induced osteogenesis. Col-I functions as a commercially available scaffold that effectively regulates the controlled release of rhBMP-2 [17], thereby preserving its bioactivity. The binding of Fn to rhBMP-2 is believed to synergistically enhance osteogenesis through integrin activation [14]. Hep and SCS, as sulfated polysaccharides, can potentiate the osteogenic activity of rhBMP-2 by interacting with its heparin binding domain [21]. A brief explanation of group names and dosage was summarized in Table 2.

C2C12 mouse myoblasts, a widely recognized cell line, were employed to assess the in vitro osteogenic potential by inducing differentiation into osteoblasts upon exposure to rhBMP-2 [43]. After stimulation with rhBMP-2, ALP activity in all groups exhibited a concentration-dependent response to rhBMP-2 (Fig. 5a). Notably, G-rhBMP-2 demonstrated significantly higher optical density values, indicating enhanced ALP induction activity even at lower concentrations (Fig. 5a). EC50 values were further analyzed to evaluate the osteoinductive activity, where higher values indicate lower bioactivity. The results confirmed the commonly observed phenomenon that G-rhBMP-2 exhibited greater in vitro activity compared to NG-rhBMP-2. Surprisingly, Col I demonstrated a negative regulatory effect on the ALP activity of NG-rhBMP-2 (Fig. 5b). We propose that this phenomenon is primarily attributed to the entanglement of dispersed type I collagen

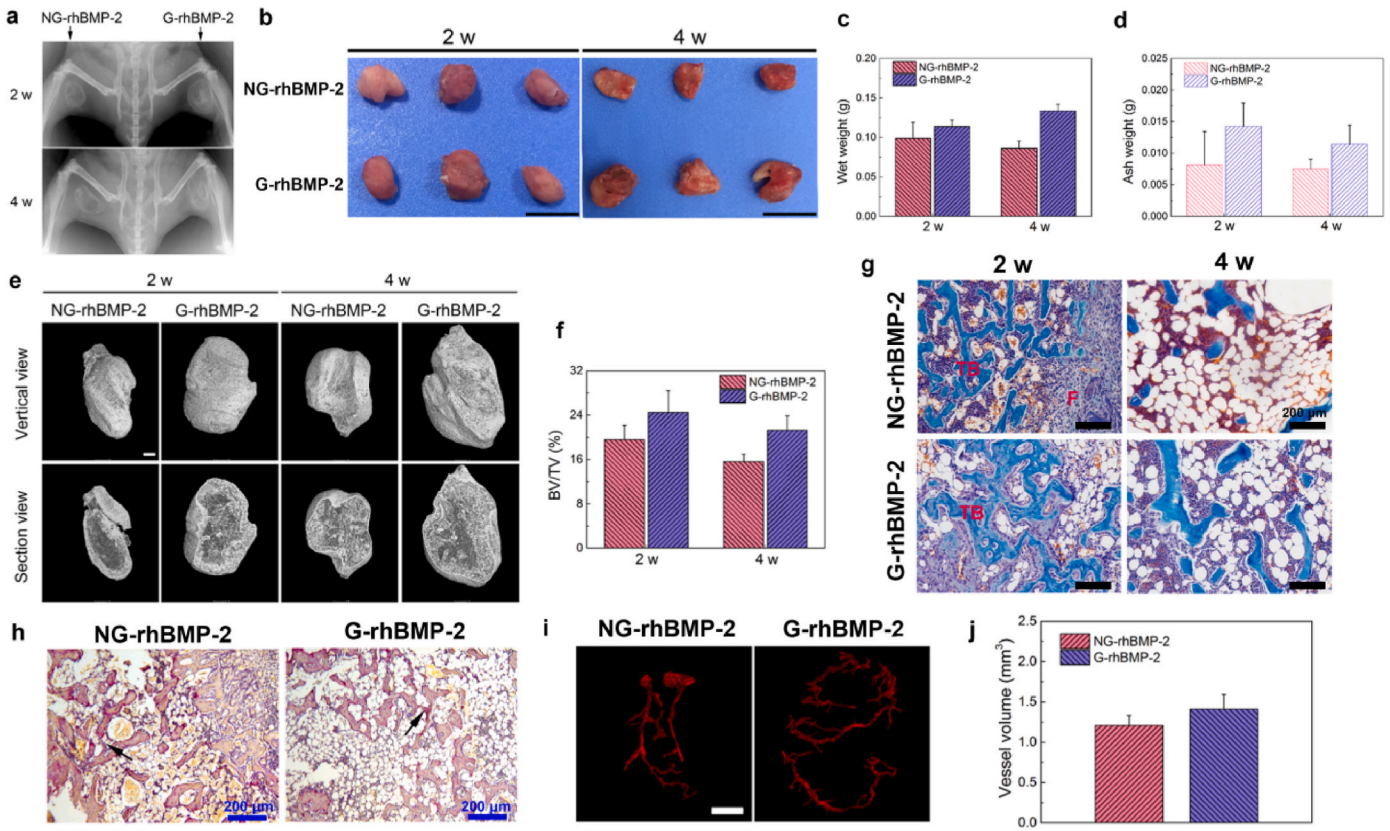

Fig. 4. The effect of glycosylation on the osteogenic activity induced by rhBMP-2. (**a**–**b**) X-ray images (a) and digital photos (b) of ectopic bone formation induced by NG-/G-rhBMP-2 at 2 weeks and 4 weeks in mice. Scale bars: 1 cm. (**c**–**d**) Wet weight (c) and ash weight (d) of ectopic bone induced by NG-/G-rhBMP-2 (n = 6). (**e**–**f**) 3D SRμCT reconstructed views of ectopic bone (e) and the percentage (f) of bone volume (BV) to total volume (TV) at 2 and 4 weeks (n = 3). RhBMP-2 amount: 10 μg. Scale bars: 1 mm. (**g**) Histological evaluation of ectopic bone sections stained with Masson's trichrome at 2 and 4 weeks. TB: trabecular bone, F: fibrous tissue. Scale bars: 200 μm. (**h**) TRAP staining of ectopic bone sections at 2 weeks. Black arrow: positive area of the osteoclasts. Scale bars: 200 μm. (**i**–**j**) 3D SRμCT reconstructed views of vessel formation (i) with quantitative analysis of vessel volume (j) (n = 3). Scale bars: 1.5 mm. G-rhBMP2 referred to glycosylated-rhBMP-2, NG-rhBMP-2 referred to non-glycosylated-rhBMP-2.

Table 2
Experimental groups in different experiments in this paper.

Experiment	Group name	Dosage
In vitro osteogenic experiment	G-rhBMP-2 or NG-rhBMP-2	0.8 μg/mL
	Col I	0.8 μg/mL NG-rhBMP-2 and 8 μg/mL Col I
	Fn	0.8 μg/mL NG-rhBMP-2 and 3.2 μg/mL Fn
	Hep	0.8 μg/mL NG-rhBMP-2 and 25.6 μg/mL Hep
	SCS	0.8 μg/mL NG-rhBMP-2 and 51.2 μg/mL SCS
In vivo ectopic bone model	LG-rhBMP-2	2 μg
	HG-rhBMP-2	20 μg
	NG-rhBMP-2	2 μg
	Col-I	2 μg NG-rhBMP-2 and 20 μg Col I
	Fn	2 μg NG-rhBMP-2 and 8 μg Fn
	Hep	2 μg NG-rhBMP-2 and 64 μg Hep
	SCS	2 μg NG-rhBMP-2 and 128 μg SCS

fibers resulting from non-specific binding to rhBMP-2, which hinders access to the active site and consequently diminishes the osteoinductive capacity. SCS had been found to enhance the ALP activity of NG-rhBMP-2; however, it remained lower than that of G-rhBMP-2 (Fig. 5b). ALP staining assay revealed that G-rhBMP-2 elicited a significantly higher level of ALP expression compared to NG-rhBMP-2. However, C2C12 cells treated with SCS and NG-rhBMP-2 exhibited a comparable blue-purple ALP protein expression to that induced by G-rhBMP-2 (Fig. 5c). In addition, the long-term effect of the chaperone molecules on matrix mineralization of C2C12 cells was assessed by Alizarin Red S staining after 14 days of culture. Similarly, Col I inhibited rhBMP-2-dependent bone mineralization (Fig. 5d). In contrast, BMP-2 combined with SCS obviously enhanced matrix mineralization relative to both G-rhBMP-2 and NG-rhBMP-2 alone, while Fn and Hep showed minimal effects (Fig. 5d).

Next, we assessed the impact of chaperone molecules on rhBMP-2-induced osteogenesis in a well-established murine ectopic bone model. In order to enhance the augmenting effect of chaperone molecules on rhBMP-2's osteogenic activity, lower concentrations of rhBMP-2 (2 μg) were employed, while a high concentration of G-rhBMP-2 (20 μg) served as a positive control. Quantitative analysis of SRμCT reconstructions revealed that in the presence of 2 μg NG-rhBMP-2, SCS had, by far, the highest mean volume of new ossified tissue relative to other control treatments containing an equal dose of NG-rhBMP-2 (Fig. 6a and b). The osteogenic potential of SCS with NG-rhBMP-2 in vivo was comparable to that of the equivalent dose of G-rhBMP-2 (LG-rhBMP-2), but lower than that of the high dose of G-rhBMP-2 (HG-rhBMP-2) (Fig. 6b). Furthermore, histological analysis using H&E staining and Masson's trichrome staining corroborated the findings obtained from SRμCT imaging (Fig. 6c). Treatment with SCS in conjunction with 2 μg NG-rhBMP-2 exhibited robust formation of trabecular bone, characterized by a more densely deposited collagen on the newly formed bone, which was visually labeled with a blue color (Fig. 6c). Our previous study

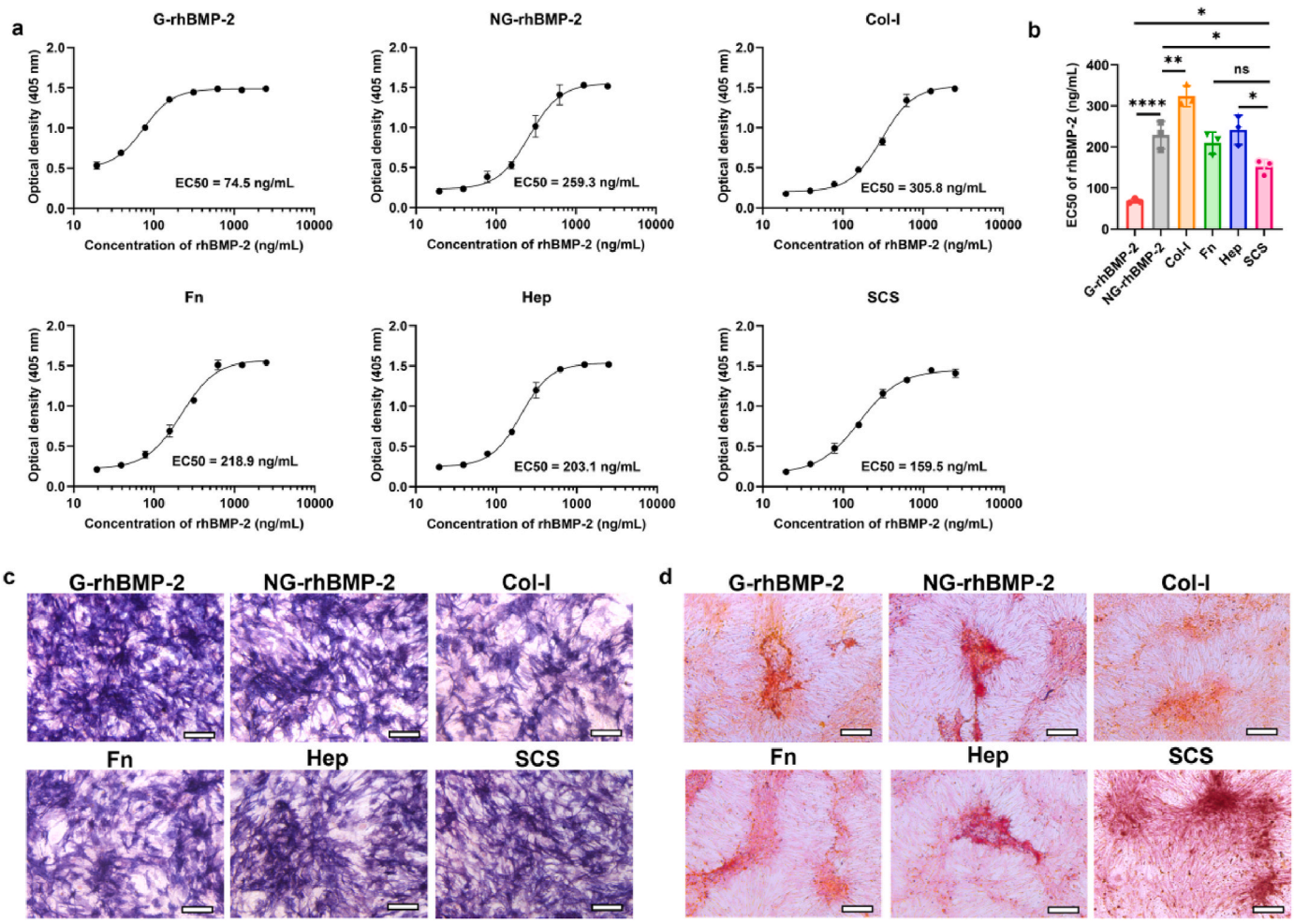

Fig. 5. Sulfated polysaccharides enhanced the osteogenic activity of NG-rhBMP-2 *in vitro*. (**a**) RhBMP-2 dose-response curves obtained by incubating C2C12 cells with rhBMP-2-and different bioactive molecules for 72 h. (**b**) Quantification of median effective concentration (EC50) values based on (a). (**c**) ALP staining of C2C12 cells cultured with rhBMP-2 (800 ng/mL) in the presence of different bioactive molecules. Scale bars, 100 μm. (**d**) Mineralization of C2C12 cells cultured with rhBMP-2 (800 ng/mL) in the presence of different bioactive molecules. Scale bars, 100 μm.

confirmed that SCS could amplify the signaling of rhBMP-2 via enhancing the binding between rhBMP-2 and BMP-2 receptors (BMPRs) and activating the phosphorylation of Smad pathway, which in turn promote the osteogenesis [21]. Additionally, previous studies have also indicated that the release kinetics of growth factor play a crucial role in inducing bone formation [44,45]. Heparin and SCS effectively modulate the in vivo release by binding to the heparin binding domain of growth factors, thereby enhancing their osteogenic efficacy. Interestingly, despite reports on Fn's affinity for BMP-2 binding, it does not exert a significant impact on BMP-2's ability to induce bone formation in vivo. This highlights the importance of improving its biological activity while considering controlled growth factor release. Together, these results suggest that the utilization of SCS as potentiators can significantly enhance the osteoinductive activity of NG-rhBMP-2, bringing it to a comparable level with G-rhBMP-2.

3. Conclusion

In this study, we successfully analyzed the structure of non-glycosylated BMP-2 protein expressed by *E. coli*, revealing a remarkable degree of consistency with the protein database. Remarkably, our findings unveiled that rhBMP-2 exhibited enhanced structural stability and osteoinductive activity in an acidic environment owing to its inherent acidity. Additionally, although the biological activity of non-glycosylated rhBMP-2 is comparatively lower than that of glycosylated rhBMP-2, we have observed a significant enhancement in its bioactivity through the introduction of chaperone molecules such as SCS. These findings provide a foundation for the rational design of rhBMP-2 stabilization and enhancement of its bioactivity, thereby improving the clinical efficacy of BMP-2.

4. Experimental section

4.1. Materials

Mouse myoblasts (C2C12) were purchased from the American Type Culture Collection. *E. Coli*-derived recombinant human bone morphogenetic protein-2 (rhBMP-2) was independently developed by our research team and produced by Shanghai Rebone Biomaterials Co. Ltd (Shanghai, China). Human 293 cell-expressed rhBMP-2 were purchased from Proteintech Group, Inc. (IL, USA). 4-nitrophenyl phosphate disodium salt hexahydrate (PNPP-Na), 1-(4, 5-dimethylthiazol-2-yl)-3, 5-diphenylformazan (MTT), and tartrate resistant acid phosphatase (TRAP) staining kit were purchased from Sigma-Aldrich (St. Louis, MO, USA). All cell-culture-related reagents were available from Gibco (Grand Island, NY, USA).

4.2. Cultivation of rhBMP-2 crystals

The crystallization of rhBMP-2 was performed as previously

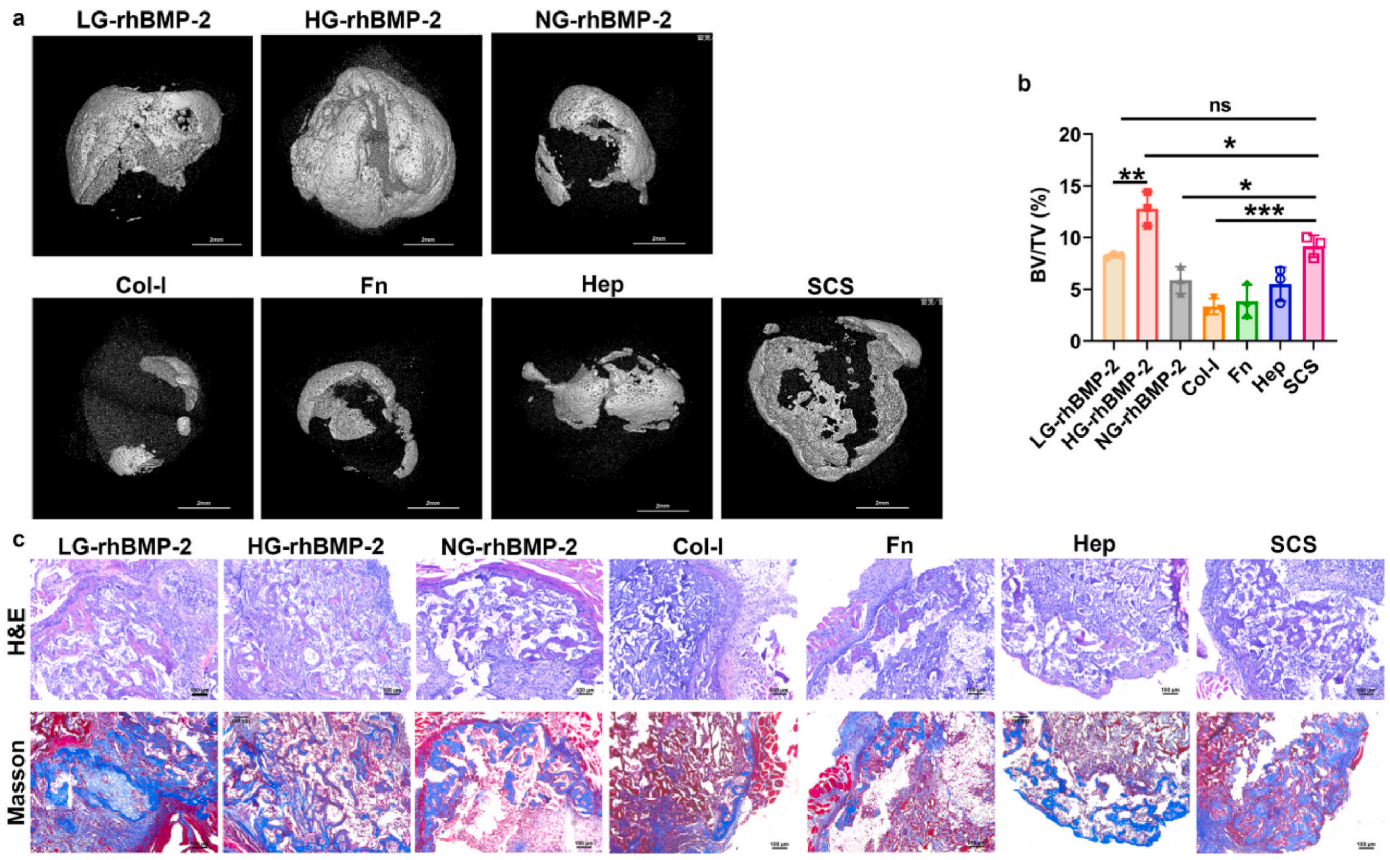

Fig. 6. Sulfated polysaccharides enhanced bone formation. (**a-b**) 3D SRμCT reconstructed views of ectopic bone (a) and the percentage (b) of bone volume (BV) to total volume (TV) at 2 weeks (n = 3). RhBMP-2 amount: 2 μg. Scale bars: 1 mm. (**c**) Histological assessment of H&E staining and Masson's trichrome staining was performed to evaluate rhBMP-2-induced ectopic bone formation with different bioactive molecules at 2 weeks. RhBMP-2 amount: 2 μg. Scale bars: 100 μm.

described [26]. Briefly, a solution containing 2.5 mg/mL rhBMP-2 in 50 mM acetate buffer (pH 3.5) was prepared. Initial crystallization trials were conducted using a 50%-screen with high concentrations of tert-butanol as the precipitant agent. However, further optimization attempts failed to refine the crystallization conditions utilizing tert-butanol alone, leading to the discovery that lithium sulfate acted as an essential co-precipitant. By employing a combination of tert-butanol at acidic pH and the hanging drop vapor diffusion method at 20 °C, delicate yet high-quality trigonal crystals were successfully obtained. The reservoir solution consisted of 50 mM citrate buffer (pH 5.4), 100 mM lithium sulfate, and 12 % (v/v) tert-butanol. Crystallization initiation involved mixing 2 μL of reservoir solution with an equal volume of protein solution.

To optimize the crystallization conditions and obtain higher quality rhBMP-2 crystals, the pH values of the reservoir solution and protein solution were systematically screened within a range of 5.0–6.0 and 3.0 to 4.0, respectively. Additionally, the protein concentration was varied from 1.0 to 3.0 mg/mL, while the lithium sulfate concentration ranged from 0 mM to 150 mM in order to identify optimal conditions for crystal formation.

4.3. Analysis of rhBMP-2 crystal structure

The crystal structure analysis of rhBMP-2 primarily involves indexing the diffraction pattern to determine central symmetry and extinction, thereby establishing the crystal's space group. The intensity of diffracted spots is converted into amplitude of the structure factor for structure determination. Molecular replacement is employed to solve phase and phase angle problems, yielding an initial structure. Subsequently, the initial protein molecular model is adjusted based on established stereochemical models such as bond length and bond angle constraints.

4.4. Preparation of rhBMP-2 solution at different formulation pH conditions

The obtained rhBMP-2 solution was stored in an acidic sodium citrate buffer. To equilibrate the pH values, the rhBMP-2 solution was first dialyzed at 4 °C with 0.02 M NaH_2PO_3 and Na_2HPO_3 buffer using a Float-a Lyzer® G2 dialysis device (Spectra, USA) for 24 h. As rhBMP-2 is easy to precipitate under alkaline condition, we re-adjusted the pH value of rhBMP-2 to 4.5, 5.5, 6.5, 7.4, and 8.5 for further study.

4.5. Particle size analysis and zeta potential measurement

For analysis the stability of rhBMP-2 at different formulation pH conditions, particle size and zeta (ζ) potential were measured using a Malvern Zetasizer Nano ZS90. Before detection, rhBMP-2 was diluted into 0.05 mg/mL in ultrapure water at different formulation pH conditions. Background reading from ultrapure water alone was subtracted from the final measurements.

4.6. Circular dichroism (CD) spectroscopy

For analysis the change of secondary structure in rhBMP-2, CD analysis was used to detect the information that affected by the formulation pH. Briefly, rhBMP-2 with a concentration of 0.1 mg/mL at different formulation pH conditions was analyzed in a range of 195~205 nm at a band width of 1 nm, scan speed of 20 nm/s and path length 1 mm. CD spectra deconvolution software CDNN was applied to

analyze the differences in secondary structure. Background reading from phosphate buffered saline (PBS) alone was subtracted from the final measurements.

4.7. Steady-state and synchronous fluorescence spectroscopy

Fluorescence spectroscopy was carried out in NaH_2PO_3 and Na_2HPO_3 solution at different formulation pH conditions on an RF-5301PC spectrofluorometer (Shimazu). Fluorescence emission spectra of rhBMP-2 were recorded from 280 to 440 nm. The excitation spectra in steady-state fluorescence spectroscopy and synchronous fluorescence spectroscopy 295 nm and 220 nm. The fluorescence data for rhBMP-2 were obtained at 25 °C using a 1 × 1 cm cuvette. All spectra were corrected for background and adjusted for dilution caused by the addition of different formulation pH solution.

4.8. Quartz crystal microbalance with dissipation (QCM-D) study

QCM-D (Q-Sense AB, Sweden) was used for in situ monitoring the surface deposition of rhBMP-2, so as to investigate the stability and aggregation of rhBMP-2 protein at different formulation pH conditions. The measurement was performed at 22 ± 0.05 °C by real time monitoring the alteration in the resonance frequency (Δf, Hz) and dissipation factor (ΔD, $\times 10^{-6}$) at 25 MHz. The diameter of the Au chip was 12 mm. Briefly, 0.02 M NaH2PO3 and Na2HPO3 buffer with different pH value was injected to obtain equilibrium with a stable baseline. RhBMP-2 (50 μg/mL) with different formulation pH conditions was then injected into the chamber at a rate of 20 μL/min until stability. The adsorbed mass, Δm (ng/cm^2), is directly calculated based on a Voigt-based viscoelastic model.

4.9. Cell viability assay

To exclude the effect of formulation pH condition on the cell viability, rhBMP-2 pre-treated with different pH conditions was anchored on the Au chips and sterilized with 75 % ethanol. Subsequently, C2C12 cells were seeded on the rhBMP-2-modified chips at a density of 2.0 × 10^4 cells/well. After the incubation period of 1 day and 3 days in Dulbecco's modified Eagle's medium (DMEM) containing 10 % FBS and 1 % penicillin-streptomycin, the media were aspirated and washed with PBS for three times. The viability of C2C12 cells treated with rhBMP-2 at different formulation pH conditions was evaluated with a MTT assay according to the manufacturer's procedure. For control, the C2C12 cells were directly seeded on the 24-well plate and incubated for the same time. All samples were tested in sextuplicate, and the results were normalized to control and expressed as mean ± SD.

4.10. Alkaline phosphatase (ALP) activity assay

ALP activity was usually measured as a marker of osteoblast differentiation. To assess the effect of formulation pH conditions on the rhBMP-2-induced osteogenic activity, C2C12 cells were seeded on the rhBMP-2 pre-treated Au chips at a density of 5.0 × 10^4 cells/well. After attaching overnight in DMEM containing 10 % FBS, 100 U/mL penicillin, 100 μg/mL streptomycin, the media were replaced with DMEM containing 2 % FBS and incubated for an additional 5 days with each day change. Subsequently, media were removed and washed several times with PBS, the cells were lysed with 200 μL of 1 % Nonidet P-40/well for 60 min. A 50 μL volume of the cell lysate was incubated with 100 μL of PNPP-Na (2 mg/mL) for 30 min at 37 °C and stopped with adding another 50 μL of 0.1 M NaOH buffer. The ALP activity was assessed by reading the OD value at 405 nm with a SpectraMax M2 microplate reader (Molecular Devices, USA). Data were normalized to the respective total protein levels using a BCA Kit (Beyotime, China). For control, the cells were incubated without the addition of rhBMP-2. All samples were tested with five replicates and expressed as mean ± SD.

For analysis of the storage stability of rhBMP-2 at different formulation pH, the stock solution was subjected to centrifugation in an ultrafiltration tube and subsequently re-dispersed in varying pH solutions at 4 °C for durations of 3, 7, 14, and 28 days. The ALP activity of the reconstituted samples was determined through co-culture with C2C12 cells over a period of 3 days.

To compare the osteoinductive activity of G-rhBMP-2 and NG-rhBMP-2, C2C12 cells were seeded in 24-well plates and allowed to adhere overnight. Subsequently, the culture medium was replaced with DMEM containing 2 % FBS and rhBMP-2 (800 ng/mL), followed by quantification of ALP activity after a 3-day incubation period.

For analysis of the effect of chaperone molecules on the NG-rhBMP-2-induced ALP expression, C2C12 cells were seeded in 96-well plates at a density of 1.0 × 10^4 cells/well and allowed to adhere overnight. Subsequently, the culture medium was replaced with DMEM containing 2 % FBS and various concentrations of rhBMP-2. After a 3-day incubation period, ALP activity was quantified. The bioactivity was assessed by fitting the experimental data to a four-parameter logistic equation model.

4.11. ALP staining

The presence of ALP was stained using a BCIP/NBT Alkaline Phosphatase Color Development Kit (Beyotime, China) according to the manufacturer's instructions. Briefly, cells were fixed with 4 % paraformaldehyde 10 min after incubation with rhBMP-2 for 3 days, washed three times with PBS and stained with staining buffer for 30 min at room temperature. Following, the samples were washed twice with deionized water. The stained samples were captured under a light microscope.

4.12. Mineralization assay

After incubation with rhBMP-2 for 10 days, the C2C12 cell layer was washed with PBS, fixed with 4 % paraformaldehyde for 10 min, stained for 30 min in 2 % Alizarin Red S (ARS, pH 4.2) solution (Beyotime, China), and gently washed twice with deionized water. The stained samples were captured under a light microscope.

4.13. Western blot analysis

The C2C12 cells were seeded in 24-well plates at a density of 1.0 × 10^5 cells/well in DMEM supplemented with 10 % FBS and incubated overnight. Subsequently, the cells were starved with DMEM containing 2 % FBS for 6 h followed by treatment with rhBMP-2 at a concentration of 0.4 μg/mL for another 6 h. For western blot analysis, total proteins were extracted from the treated C2C12 cells using RIPA lysis buffer supplemented with 1 mM PMSF. An equal number of proteins was separated by an SDS-polyacrylamide gel (8 %) and transferred to a nitrocellulose membrane (Millipore, USA) via electrotransfer. The membranes were then blocked using a solution of 5 % BSA and subsequently incubated overnight at 4 °C with primary antibodies against p-Smad1/5/9, Smad1/5/9, Runx2, and GAPDH (dilution: 1:1000; CST). This was followed by incubation with their corresponding secondary HRP-conjugated antibodies (dilution: 1:1000; CST). Protein signals were detected using the ECL chemiluminescent system (Tanon, China).

4.14. Quantitative RT-PCR analysis

The gene expression levels were determined using a CFX96 Touch™ PCR Detection System (Bio-Rad, USA) through real-time reverse transcription PCR. C2C12 cells were seeded at a density of 5.0 × 10^4 cells/well in DMEM (10 % FBS) and allowed to adhere overnight in 24-well plates. Subsequently, the medium was replaced with DMEM (2 % FBS) supplemented with G-rhBMP-2 and NG-rhBMP-2 for continuous culture periods of 3 days and 7 days, were extracted from C2C12 cells using an RNAiso Plus TRIzol reagent (Takara, Japan), followed by reverse

transcription into complementary DNA (cDNA) using the PrimeScript™ RT reagent kit according to the manufacturer's instructions. Finally, qPCR was performed using TB Green® Premix Ex Taq™ (Takara, Japan). The primer sequences used in this study are listed in Table S3. Glyceraldehyde-3-phosphate dehydrogenase (GAPDH) was employed as a reference gene. Results were analyzed using the comparative Ct ($2^{-\Delta\Delta Ct}$) method and expressed as fold changes relative to the control group. All samples were assayed in triplicate.

4.15. Ectopic bone formation experiment

Male C57BL/6 mice (6 weeks old, jsj-lab. Shanghai, China) were utilized for in vivo assessment of osteogenesis activity. Following anesthesia with an intraperitoneal injection of sodium pentobarbital (0.08 mg/g body weight), gelatin sponge containing rhBMP-2 was implanted into the leg muscle pouches of the mice. X-ray imaging was performed to evaluate the size of ectopic bones after 2 or 4 weeks of implantation. Subsequently, the mice were euthanized using an overdose injection of pentobarbital to obtain specimens. The fresh ectopic bones were promptly photographed using a digital camera. The weights of all samples were measured in wet and ash states (incinerated at 800 °C in a muffle).

4.16. Synchrotron radiation-based micro-computed tomography (SRμCT)

After administering an overdose injection of pentobarbital, the thoracic cavity of mice was opened and a needle was inserted into the left ventricle to flush out the blood with heparinized saline solution. Subsequently, Microfil reagent (MV-120, Flow Tech. Inc., USA) was injected into the vasculature. The mice were then stored at 4 °C overnight to allow for gelation of the Microfil substance. The ectopic bones were retrieved and fixed in 4 % paraformaldehyde before being imaged using SRμCT to determine their volume. Following this, decalcification of the ectopic bones was carried out using 15 % neutral EDTA, and angiography images were obtained using SRμCT as well. All SRμCT measurements were performed at beamline BL13B of Shanghai Synchrotron Radiation Facility (SSRF, Shanghai, China), with a voxel size set at 9 μm. Brucker software was utilized for visualizing the three-dimensional structure based on slice images.

4.17. Histology analysis

For histological analysis, the ectopic bones were fixed with formaldehyde solution for a duration of 3 days. Subsequently, they were decalcified using a 10 % neutral EDTA solution and then embedded in paraffin after undergoing dehydration through a graded series of alcohol. Serial sections with a thickness of 4.5 μm were stained utilizing hematoxylin & eosin (H&E) as well as Masson trichrome techniques to visualize tissue structures and extracellular matrix components respectively. Tartrate resistant acid phosphatase (TRAP) staining was conducted with a Leukocyte Acid Phosphatase Kit from Sigma following the manufacturer's instructions to identify osteoclasts. Additionally, immunostainings targeting CD31 were conducted to specifically detect blood vessels within the ectopic bone samples. Briefly, the sections were incubated overnight at 4 °C with a primary antibody against mouse CD31 (diluted 1:100; Abcam, Cambridge, UK) after pre-blocking with 10 % goat serum for 1 h at room temperature. Subsequently, they were incubated with an HRP-conjugated secondary antibody (diluted 1:250; Abcam, Cambridge, UK). Finally, the CD31 positive expression was labeled using the DAB substrate. The sections were then treated with hematoxylin and mounted. The stained samples were captured under a light microscope and the vessel area was quantified using Image J software.

4.18. Statistical analysis

The quantitative data were presented as the mean ± SD and analyzed using Origin 8.5 (OriginLab Corp., Northhampton, MA, USA). Statistical comparisons were conducted through one-way analysis of variance (ANOVA) followed by Tukey's post hoc test. Statistical significance was achieved at a confidence level exceeding 95 % ($P < 0.05$).

Ethics approval

All procedures were approved by the Animal Research Committee of East China University of Science and Technology. The ethical approval number was ECUST-21010.

Declaration of competing interest

The authors declare that they have no known competing financial interests or personal relationships that could have appeared to influence the work reported in this paper.

CRediT authorship contribution statement

Yuanman Yu: Writing – original draft, Visualization, Formal analysis, Data curation, Conceptualization. **Rui Chen:** Writing – review & editing, Visualization, Methodology. **Xinye Chen:** Writing – review & editing, Methodology. **Jing Wang:** Writing – review & editing, Supervision, Project administration, Funding acquisition. **Changsheng Liu:** Project administration, Funding acquisition.

Acknowledgements

This research was supported by the Basic Science Center Program of National Natural Science Foundation of China (No.T2288102), the Key Program of the National Natural Science Foundation of China (No. 32230059), the National Natural Science Foundation of China (No. 32101086), the National Postdoctoral Program for Innovative Talents (BX2021101), and the China Postdoctoral Science Foundation Funded Project (2021M701192), Fundamental Research Funds for the Central Universities (JKD01221507), and the Foundation of Frontiers Science Center for Materiobiology and Dynamic Chemistry (JKVD1211002).

Appendix A. Supplementary data

Supplementary data to this article can be found online at https://doi.org/10.1016/j.bioactmat.2024.04.018.

References

[1] J.M. Wozney, V. Rosen, A.J. Celeste, L.M. Mitsock, E.A. Wang, Novel regulators of bone formation: molecular clones and activities, Science 242 (1988) 1528–1534. https://10.1126/science.3201241.
[2] A. Yamaguchi, Recombinant human bone morphogenetic protein-2 stimulates osteoblastic maturation and inhibits myogenic differentiation in vitro, J. Cell Biol. 113 (1991) 681–687, https://doi.org/10.1083/jcb.113.3.681.
[3] C.A. Tannoury, H.S. An, Complications with the use of bone morphogenetic protein 2 (BMP-2) in spine surgery, Spine J. 14 (2014) 552–559, https://doi.org/10.1016/j.spinee.2013.08.060.
[4] O.P. Gautschi, S.P. Frey, R. Zellweger, Bone morphogenetic proteins in clinical applications, ANZ J. Surg. 77 (2010) 626–631, https://doi.org/10.1111/j.1445-2197.2007.04175.x.
[5] D.I. Israel, J. Nove, K.M. Kerns, I.K. Moutsatsos, R.J. Kaufman, Expression and characterization of bone morphogenetic protein-2 in Chinese hamster ovary cells, Growth Factors 7 (2009) 139–150, https://doi.org/10.3109/08977199209046403.
[6] L.F. Vallejo, M. Brokelmann, S. Marten, S. Trappe, J. Cabrera-Crespo, A. Hoffmann, G. Gross, H.A. Weich, U. Rinas, Renaturation and purification of bone morphogenetic protein-2 produced as inclusion bodies in high-cell-density cultures of recombinant Escherichia coli, J. Biotechnol. 94 (2002) 185–194, https://doi.org/10.1016/S0168-1656(01)00425-4.
[7] T.K. Sampath, J.E. Coughlin, R.M. Whetstone, D. Banach, C. Corbett, R.J. Ridge, E. Ozkaynak, H. Oppermann, D.C. Rueger, Bovine osteogenic protein is composed

of dimers of OP-1 and BMP-2A, two members of the transforming growth factor-beta superfamily, J. Biol. Chem. 265 (1990) 13198–13205, https://doi.org/10.1016/S0021-9258(19)38285-7.
[8] W. Wei, Instability, stabilization, and formulation of liquid protein pharmaceuticals, Int. J. Pharm. 185 (1999) 129–188, https://doi.org/10.1016/S0378-5173(99)00152-0.
[9] E.Y. Chi, S. Krishnan, T.W. Randolph, J.F. Carpenter, Physical stability of proteins in aqueous solution: mechanism and driving forces in nonnative protein aggregation, Pharm. Res. (N. Y.) 20 (2003) 1325–1336, https://doi.org/10.1023/A:1025771421906.
[10] Y. Sun, D. Devore, X. Ma, Y. Yuan, J. Kohn, J. Qian, Promotion of dispersion and anticancer efficacy of hydroxyapatite nanoparticles by the adsorption of fetal bovine serum, J. Nanoparticle Res. 21 (2019) 267, https://doi.org/10.1007/s11051-019-4711-2.
[11] M. Bucciantini, E. Giannoni, F. Chiti, F. Baroni, N. Taddei, G. Ramponi, C. M. Dobson, M. Stefani, Inherent toxicity of aggregates implies a common mechanism for protein misfolding diseases, Nature 416 (2002) 507–511, https://doi.org/10.1038/416507a.
[12] C.J. Roberts, Protein aggregation and its impact on product quality, Curr. Opin. Biotechnol. 30 (2014) 211–217, https://doi.org/10.1016/j.copbio.2014.08.001.
[13] W. Wang, C.J. Roberts, Protein aggregation – mechanisms, detection, and control, Int. J. Pharm. 550 (2018) 251–268, https://doi.org/10.1016/j.ijpharm.2018.08.043.
[14] M.M. Martino, F. Tortelli, M. Mochizuki, S. Traub, D. Ben-David, G.A. Kuhn, R. Müller, E. Livne, S.A. Eming, J.A. Hubbell, Engineering the growth factor microenvironment with fibronectin domains to promote wound and bone tissue healing, Sci. Transl. Med. 3 (2011), https://doi.org/10.1126/scitranslmed.3002614, 100ra89-100ra89.
[15] V. Llopis-Hernández, M. Cantini, C. González-García, Z.A. Cheng, J. Yang, P. M. Tsimbouri, A.J. García, M.J. Dalby, M. Salmerón-Sánchez, Material-driven fibronectin assembly for high-efficiency presentation of growth factors, Sci. Adv. 2 (2016) e1600188, https://doi.org/10.1126/sciadv.1600188.
[16] S. Rasi Ghaemi, B. Delalat, X. Cetó, F.J. Harding, J. Tuke, N.H. Voelcker, Synergistic influence of collagen I and BMP 2 drives osteogenic differentiation of mesenchymal stem cells: a cell microarray analysis, Acta Biomater. 34 (2016) 41–52, https://doi.org/10.1016/j.actbio.2015.07.027.
[17] P.S. Briquez, H.-M. Tsai, E.A. Watkins, J.A. Hubbell, Engineered bridge protein with dual affinity for bone morphogenetic protein-2 and collagen enhances bone regeneration for spinal fusion, Sci. Adv. 7 (2021) eabh4302, https://doi.org/10.1126/sciadv.abh4302.
[18] R. Ruppert, E. Hoffmann, W. Sebald, Human bone morphogenetic protein 2 contains a heparin-binding site which modifies its biological activity, Eur. J. Biochem. 237 (1996) 295–302, https://doi.org/10.1111/j.1432-1033.1996.0295n.x.
[19] S. Kanzaki, W. Ariyoshi, T. Takahashi, T. Okinaga, T. Kaneuji, S. Mitsugi, K. Nakashima, T. Tsujisawa, T. Nishihara, Dual effects of heparin on BMP-2-induced osteogenic activity in MC3T3-E1 cells, Pharmacol. Rep. 63 (2011) 1222–1230, https://doi.org/10.1016/S1734-1140(11)70642-9.
[20] R.A.A. Smith, S. Murali, B. Rai, X. Lu, Z.X.H. Lim, J.J.L. Lee, V. Nurcombe, S. M. Cool, Minimum structural requirements for BMP-2-binding of heparin oligosaccharides, Biomaterials 184 (2018) 41–55, https://doi.org/10.1016/j.biomaterials.2018.08.056.
[21] Y. Yu, R. Chen, Y. Yuan, J. Wang, C. Liu, Affinity-selected polysaccharide for rhBMP-2-induced osteogenesis via BMP receptor activation, Appl. Mater. Today 20 (2020) 100681, https://doi.org/10.1016/j.apmt.2020.100681.
[22] C. Liu, J. Lin, Q. Jiangchao, Y. Yuan, Optimized DNA Sequences Encoding Recombinant Human Bone Morphogenetic Protein-2 (rhBMP-2), Preparation Method and the Uses Thereof, 7, U.S. Patent No., 2011, 947,821. 24 May.
[23] H. Matsumoto, Y. Koyama, A. Tanioka, Interaction of proteins with weak amphoteric charged membrane surfaces: effect of pH, J. Colloid Interface Sci. 264 (2003) 82–88, https://doi.org/10.1016/S0021-9797(03)00417-X.
[24] Q. Han, S.J. Brown, C.J. Drummond, T.L. Greaves, Protein aggregation and crystallization with ionic liquids: insights into the influence of solvent properties, J. Colloid Interface Sci. 608 (2022) 1173–1190, https://doi.org/10.1016/j.jcis.2021.10.087.
[25] D. Hekmat, Large-scale crystallization of proteins for purification and formulation, Bioproc. Biosyst. Eng. 38 (2015) 1209–1231, https://doi.org/10.1007/s00449-015-1374-y.
[26] C. Scheufler, W. Sebald, M. Hülsmeyer, Crystal structure of human bone morphogenetic protein-2 at 2.7 Å resolution11Edited by R. Huber, J. Mol. Biol. 287 (1999) 103–115, https://doi.org/10.1006/jmbi.1999.2590.
[27] G. Gieseler, I. Pepelanova, L. Stuckenberg, L. Villain, V. Nölle, U. Odenthal, S. Beutel, U. Rinas, T. Scheper, Purification of bone morphogenetic protein-2 from refolding mixtures using mixed-mode membrane chromatography, Appl. Microbiol. Biotechnol. 101 (2017) 123–130, https://doi.org/10.1007/s00253-016-7784-1.
[28] J. Aslam, I. Hussain Lone, F. Ansari, A. Aslam, R. Aslam, M. Akram, Molecular binding interaction of pyridinium based gemini surfactants with bovine serum albumin: insights from physicochemical, multispectroscopic, and computational analysis, Spectrochim. Acta Part A Mol. Biomol. Spectrosc. 250 (2021) 119350, https://doi.org/10.1016/j.saa.2020.119350.
[29] S. Zhang, R. Gan, L. Zhao, Q. Sun, H. Xiang, X. Xiang, G. Zhao, H. Li, Unveiling the interaction mechanism of alogliptin benzoate with human serum albumin: insights from spectroscopy, microcalorimetry, and molecular docking and molecular dynamics analyses, Spectrochim. Acta Part A Mol. Biomol. Spectrosc. 246 (2021) 119040, https://doi.org/10.1016/j.saa.2020.119040.
[30] R. Mondal, N. Ghosh, S. Mukherjee, Contrasting effects of pH on the modulation of the structural integrity of hemoglobin induced by sodium deoxycholate, Phys. Chem. Chem. Phys. 18 (2016) 30867–30876, https://doi.org/10.1039/c6cp05216a.
[31] I. Jha, P. Attri, P. Venkatesu, Unexpected effects of the alteration of structure and stability of myoglobin and hemoglobin in ammonium-based ionic liquids, Phys. Chem. Chem. Phys. Pccp 16 (2014) 5514–5526, https://doi.org/10.1039/C3CP54398F.
[32] M.S. Rahman, N. Akhtar, H.M. Jamil, R.S. Banik, S.M. Asaduzzaman, TGF-β/BMP signaling and other molecular events: regulation of osteoblastogenesis and bone formation, Bone Res 3 (2015) 15005, https://doi.org/10.1038/boneres.2015.5.
[33] K. Irie, C. Alpaslan, K. Takahashi, Y. Kondo, N. Izumi, Y. Sakakura, E. Tsuruga, T. Nakajima, S. Ejiri, H. Ozawa, T. Yajima, Osteoclast differentiation in ectopic bone formation induced by recombinant human bone morphogenetic protein 2 (rhBMP-2), J. Bone Miner. Metabol. 21 (2003) 363–369, https://doi.org/10.1007/s00774-003-0430-x.
[34] R.Y. Kim, J.H. Oh, B.S. Lee, Y.-K. Seo, S.J. Hwang, I.S. Kim, The effect of dose on rhBMP-2 signaling, delivered via collagen sponge, on osteoclast activation and in vivo bone resorption, Biomaterials 35 (2014) 1869–1881, https://doi.org/10.1016/j.biomaterials.2013.11.029.
[35] A.P. Kusumbe, S.K. Ramasamy, R.H. Adams, Coupling of angiogenesis and osteogenesis by a specific vessel subtype in bone, Nature 507 (2014) 323–328, https://doi.org/10.1038/nature13145.
[36] M.M.L. Deckers, R.L. van Bezooijen, G. van der Horst, J. Hoogendam, C. van der Bent, S.E. Papapoulos, C.W.G.M. Löwik, Bone morphogenetic proteins stimulate angiogenesis through osteoblast-derived vascular endothelial growth factor A, Endocrinology 143 (2002) 1545–1553, https://doi.org/10.1210/endo.143.4.8719.
[37] W.-C. Chen, C.-H. Chung, Y.-C. Lu, M.-H. Wu, P.-H. Chou, J.-Y. Yen, Y.-W. Lai, G.-S. Wang, S.-C. Liu, J.-K. Cheng, Y.-J. Wu, H.-I. Yeh, L.-Y. Wang, S.-W. Wang, BMP-2 induces angiogenesis by provoking integrin α6 expression in human endothelial progenitor cells, Biochem. Pharmacol. 150 (2018) 256–266, https://doi.org/10.1016/j.bcp.2018.02.021.
[38] H.B. Pearson, D.E. Mason, C.D. Kegelman, L. Zhao, J.H. Dawahare, M.A. Kacena, J. D. Boerckel, Effects of bone morphogenetic protein-2 on neovascularization during large bone defect regeneration, Tissue Eng. 25 (2019) 1623–1634, https://doi.org/10.1089/ten.tea.2018.0326.
[39] M. Geiger, R.H. Li, W. Friess, Collagen sponges for bone regeneration with rhBMP-2, Adv. Drug Deliv. Rev. 55 (2003) 1613–1629, https://doi.org/10.1016/j.addr.2003.08.010.
[40] T.-M. De Witte, L.E. Fratila-Apachitei, A.A. Zadpoor, N.A. Peppas, Bone tissue engineering via growth factor delivery: from scaffolds to complex matrices, Regen. Biomater. 5 (2018) 197–211, https://doi.org/10.1093/rb/rby013.
[41] V. Hintze, S.A. Samsonov, M. Anselmi, S. Moeller, J. Becher, M. Schnabelrauch, D. Scharnweber, M.T. Pisabarro, Sulfated glycosaminoglycans exploit the conformational plasticity of bone morphogenetic protein-2 (BMP-2) and alter the interaction profile with its receptor, Biomacromolecules 15 (2014) 3083–3092, https://doi.org/10.1021/bm5006855.
[42] C. Mücksch, H.M. Urbassek, Adsorption of BMP-2 on a hydrophobic graphite surface: a molecular dynamics study, Chem. Phys. Lett. 510 (2011) 252–256, https://doi.org/10.1016/j.cplett.2011.05.036.
[43] T. Katagiri, A. Yamaguchi, M. Komaki, E. Abe, N. Takahashi, T. Ikeda, V. Rosen, J. M. Wozney, A. Fujisawa-Sehara, T. Suda, Bone morphogenetic protein-2 converts the differentiation pathway of C2C12 myoblasts into the osteoblast lineage, J. Cell Biol. 127 (1994) 1755–1766, https://doi.org/10.1083/jcb.127.6.1755.
[44] D.H.R. Kempen, L. Lu, T.E. Hefferan, L.B. Creemers, A. Maran, K.L. Classic, W.J. A. Dhert, M.J. Yaszemski, Retention of in vitro and in vivo BMP-2 bioactivities in sustained delivery vehicles for bone tissue engineering, Biomaterials 29 (2008) 3245–3252, https://doi.org/10.1016/j.biomaterials.2008.04.031.
[45] K. V Brown, B. Li, T. Guda, D.S. Perrien, S.A. Guelcher, J.C. Wenke, Improving bone formation in a rat femur segmental defect by controlling bone morphogenetic protein-2 release, Tissue Eng. 17 (2011) 1735–1746, https://doi.org/10.1089/ten.tea.2010.0446.